

An efficient and generalized consistency correction method for weakly-compressible SPH

Yaru Ren^{a,b}, Pengzhi Lin^a, Chi Zhang^{b,c}, Xiangyu Hu^{b,*}

^a*State Key Laboratory of Hydraulics and Mountain River Engineering, Sichuan University, Chengdu, Sichuan, China*

^b*Department of Mechanical Engineering, Technical University of Munich 85748 Garching, Germany*

^c*Huawei Technologies Munich Research Center 80992 Munich, Germany*

Abstract

In this paper, a new efficient and generalized consistency correction method for weakly-compressible smoothed particle hydrodynamics is proposed and successfully implemented in the simulation of violent free-surface flow exhibiting breaking and impact events for the first time. It's well known that the original kernel gradient correction (KGC) encounters numerical instability resulting from matrix inversion. The present method remedies this issue by introducing a weighted average of the KGC matrix and the identity matrix, other than directly applying KGC matrix, to achieve numerical stability meanwhile decrease numerical dissipation. To ensure momentum conservation, the correction is implemented in a particle-average pattern by rewriting the the pressure term of the Riemann solution. Furthermore, the proposed weighted KGC scheme is incorporated into the dual-criteria time-stepping framework developed by Zhang et al. (2020) [1] to achieve optimized com-

*Corresponding author.

Email address: xiangyu.hu@tum.de (Xiangyu Hu)

putational efficiency. A set of numerical examples in both two- and three-dimensions are investigated to demonstrate that the present method can significantly reduce numerical dissipation meanwhile exhibit a smooth pressure field for general free-surface flows.

Keywords: SPH, kernel gradient correction, free-surface flow, numerical stability

1. Introduction

In the past decades, particle-based methods have attracted more and more attentions thanks to their Lagrangian nature which can easily handle large material deformations and capture moving surfaces and interfaces. As one of the key examples, smoothed particle hydrodynamics (SPH) [2, 3, 4, 5] has experienced tremendous developments in engineering applications, such as those of coastal and ocean engineering [3, 6], astrophysics [7], geotechnical engineering [8], and so on. While recognized as a promising potential in coastal and ocean engineering, the SPH method encounters excessive numerical dissipation in the simulation of the wave propagation [9, 10], leading to the over damping of mechanical energy [11, 12].

To remedy this issue, several algorithms have been developed in the literature and they are generally categorized into three groups, i.e. introducing adaptive numerical dissipation, increasing the smoothing length and applying kernel gradient correction (KGC). The adaptive numerical dissipation scheme, including δ -SPH [13, 14] and Riemann-SPH [15, 16], has demonstrated its ability to improve the energy conservation while still exhibit over damping of mechanical energy in wave dynamics. Increasing the smoothing

Table 1: Different KGC schemes in literature.

No.	Corrected gradient form ¹	Momentum Conservation	Numerical Stability
S1	$\tilde{\nabla}_i W_{ij} = \mathbf{B}_i \nabla_i W_{ij}$	No	No
S2	$\tilde{\nabla}_i W_{ij} = \frac{1}{2} (\mathbf{B}_i + \mathbf{B}_j) \nabla_i W_{ij}$	Yes	No
S3	$\tilde{\nabla}_i W_{ij} = \frac{1}{2} (\mathbf{A}_i + \mathbf{A}_j)^{-1} \nabla_i W_{ij}$	Yes	No
S4	$\tilde{\nabla}_i W_{ij} = \text{diag}(\mathbf{B}_i) \nabla_i W_{ij}$	No	No

¹ \mathbf{B} the correction matrix ($\mathbf{B} = \mathbf{A}^{-1}$), ∇W the original kernel gradient and $\tilde{\nabla} W$ the corrected kernel gradient. Refer to Sections 2 and 3 for more details.

length is a simple and effective approach for reducing the numerical dissipation in the weakly-compressible SPH (WCSPH) method. Typically, the smoothing length is set to be twice the initial particle spacing to achieve satisfactory results, as reported in the literature [17, 14, 16]. However, this approach also incurs a significantly higher computational cost, particularly in 3D simulations.

The KGC scheme, also known as renormalized scheme, was first investigated by Randles et al. [18]. Since then, it has been extensively studied and incorporated into different SPH methods to improve numerical accuracy and consistency [19, 20, 9, 21]. Several formulations have been proposed in the literature concerning the proper implementation of the KGC, which are briefly summarized in Table 1. Specifically, scheme S1, encounters two drawbacks [22, 21], viz, the momentum non-conservation due to its asymmetric form and the numerical instability as the ill-conditioned matrix inversion of particles close to boundary. To address these issues, Vila [23] suggested a symmetric version as scheme S2 which preserves momentum conservation

while is not first-order consistent any more. Guilcher et al.[9] applied this scheme to wave dynamics and achieved improved performance in predicting wave propagation. Zago et al. [12] pointed out that this scheme exhibit numerical instability in the proximity of the free surface when a smaller artificial viscosity coefficient is applied. To address this instability, Zago et al. [12] proposed a new symmetric version by first obtaining the particle average matrix and then its inverse as scheme S3. Even though scheme S3 exhibits improved robust features, it requires calculating the inverse matrix for every particle pair, introducing extra computational efforts [24] compared with scheme S2. Zhang and Liu [25] introduced scheme S4 by assuming that the correction matrix is diagonally dominant and therefore the contributions from other directions can be neglected to avoid the correction matrix inversion. However, this assumption is not reasonable for violent free-surface flow exhibiting breaking and impact events, leading to the loss of accuracy. Instead of applying a KGC scheme to all fluid particles, Zago et al. [12] achieved stable simulation by not applying the correction to particles with incomplete supports or distorted configurations. They introduced a cut-off threshold based on the determinant value of the correction matrix to detect particles with matrix deficiencies. One main weakness is that the tunable threshold requires careful numerical calibrations and its values usually are case dependent, in particular for modeling violent free-surface flows. Therefore, introducing KGC to increase accuracy and decrease numerical dissipation without inducing numerical instability for general free surface flows is still not addressed in the literature.

In this paper, we focus on the KGC scheme and propose a generalized

and consistent weighted KGC (WKGC) for WCSPH to decrease the numerical dissipation meanwhile guarantee numerical stability for general free surface flows. Instead of directly applying the KGC or introducing a cut-off threshold, the present method introduces a weighted average of the original KGC matrix and the identity matrix to address the induced numerical instability. Therefore, the particles with ill-conditioned correction matrices are corrected by diagonally dominant matrices to ensure numerical stability. Then, the correction is implemented in a particle-average pattern by rewriting the the pressure term of the Riemann solution to ensure momentum conservation. Also, the WKGC is incorporated into a dual-criteria time stepping framework, taking into account computational efficiency. Two- and three-dimensional cases, including standing wave, oscillation drop, dam break and 3D wave-structure interaction, are investigated to test the accuracy and stability of the method.

2. Weakly compressible SPH method

2.1. Governing equation

The governing equation in the lagrangian framework for viscous flows includes the mass and momentum conservation equations read:

$$\begin{cases} \frac{d\rho}{dt} = -\rho\nabla \cdot \mathbf{v} \\ \frac{d\mathbf{v}}{dt} = -\frac{1}{\rho}\nabla p + \mathbf{a}_\nu + \mathbf{g}, \end{cases} \quad (1)$$

where ρ the fluid density, \mathbf{v} the velocity, p the pressure, \mathbf{g} the gravitational acceleration, \mathbf{a}_ν the acceleration due to the viscous force and $\frac{d}{dt} = \frac{\partial}{\partial t} + \mathbf{v} \cdot \nabla$ refers to the material derivative.

To model the incompressible flow with the weakly-compressible assumption, the pressure and density are related through an artificial equation of state (Eos)

$$p = c_0^2(\rho - \rho_0), \quad (2)$$

where ρ_0 the initial density and c_0 the artificial speed of sound. With the weakly-compressible assumption, the density variation maintains below 1% by setting $c_0 = 10U_{max}$ with U_{max} denoting the anticipated maximum fluid speed.

2.2. Riemann-SPH method

To discretize the system of Eq.(1), we adopt the Riemann-SPH method [15] where the continuity and momentum equations are discretized as

$$\begin{cases} \frac{d\rho_i}{dt} = 2\rho_i \sum_j (\mathbf{v} - \mathbf{v}^*) \cdot V_j \nabla_i W_{ij} \\ \frac{d\mathbf{v}_i}{dt} = -2 \sum_j \frac{P^*}{\rho_i} V_j \nabla_i W_{ij} + 2 \sum_j \frac{\nu}{\rho_i} \mathbf{v}_{ij} V_j \nabla_i W_{ij} + \mathbf{g}_i, \end{cases} \quad (3)$$

where V_j is the particle volume, $\mathbf{v}_{ij} = \mathbf{v}_i - \mathbf{v}_j$ the relative velocity. ν the fluid kinetic viscosity and $\nabla_i W_{ij} = \frac{\partial W}{\partial \mathbf{r}_{ij}} \mathbf{e}_{ij}$ with $\mathbf{e}_{ij} = \frac{\mathbf{r}_{ij}}{|\mathbf{r}_{ij}|}$. Note that, \mathbf{v}^* and P^* are the solutions of the Riemann problem constructed along the interacting line of a particle pair pointed from particle i to j . The left and the right states of the Riemann problem are defined

$$\begin{cases} (\rho_L, U_L, P_L, c_L) = (\rho_i, -\mathbf{v}_i \cdot \mathbf{e}_{ij}, p_i, c_i) \\ (\rho_R, U_R, P_R, c_R) = (\rho_j, -\mathbf{v}_j \cdot \mathbf{e}_{ij}, p_j, c_j), \end{cases} \quad (4)$$

To solve the Riemann problem, we apply the linearised Riemann solver with a dissipation limiter [15] and obtain

$$\begin{cases} \mathbf{v}^* = \frac{1}{2}(\mathbf{v}_i + \mathbf{v}_j) - (U^* - \frac{1}{2}(U_L + U_R)) \cdot \mathbf{e}_{ij} \\ U^* = \frac{(\rho_L c_L U_L + \rho_R c_R U_R + P_L - P_R)}{\rho_L c_L + \rho_R c_R} \\ P^* = \frac{(\rho_L c_L P_R + \rho_R c_R P_L + \rho_L c_L \rho_R c_R (U_L - U_R) \beta)}{\rho_L c_L + \rho_R c_R}, \end{cases} \quad (5)$$

where $\beta = \min(3\max((U_L - U_R)/((c_L - c_R)/(\rho_L + \rho_R)), 0.0), 1.0)$ is the low-dissipation limiter.

3. Weighted kernel gradient correction

In this part, the WKGC scheme is presented in detail with its implementation in Riemann-SPH and dual-criteria time stepping frameworks.

3.1. Weighted KGC scheme

In SPH, the kernel approximation of the gradient of a field reads

$$\nabla f(\mathbf{r}) = \int_{\Omega} (f(\mathbf{r}') - f(\mathbf{r})) \nabla W d\mathbf{r}'. \quad (6)$$

Then we can conduct the Taylor expansion and have

$$\nabla f(\mathbf{r}) = \nabla f(\mathbf{r}) \int_{\Omega} (\mathbf{r}' - \mathbf{r}) \otimes \nabla W d\mathbf{r}' + O(h^2). \quad (7)$$

It is easy to conclude that Eq.(7) achieves 1-order consistency if the following condition is satisfied

$$\int_{\Omega} (\mathbf{r}' - \mathbf{r}) \otimes \nabla W d\mathbf{r}' = \mathbf{I}. \quad (8)$$

In term of particle approximation [26], Eq.(8) can be rewritten as

$$\sum_j \mathbf{r}_{ji} \otimes \nabla_i W_{ij} V_j = \mathbf{I}. \quad (9)$$

However, Eq.(9) can't be fulfilled for the irregular particle distribution or particles close to the boundary. Therefore, in the KGC scheme, a corrected matrix \mathbf{B}_i is introduced to modify Eq.(9) as

$$\mathbf{B}_i \sum_j \mathbf{r}_{ji} \otimes \nabla_i W_{ij} V_j = \mathbf{I}, \quad (10)$$

where

$$\mathbf{B}_i = \left(\sum_j \mathbf{r}_{ji} \otimes \nabla_i W_{ij} V_j \right)^{-1} = (\mathbf{A}_i)^{-1} \quad (11)$$

The KGC scheme can improve computational accuracy and achieve 1st-order consistency both for irregular particle distributions and particles close to the boundary. While it may violate the anti-symmetric property of the SPH discretization, indicating a non-conservation form of momentum. Moreover, the KGC suffers instability when the condition number of the matrix \mathbf{A} is very large [27]. More precisely, when the matrix determinant tends to be zero, a small disturbance may result in large changes in the inverse matrix and induces numerical instability. As discussed in Section 1, the existing variants of the KGC still suffer from the numerical instability issue.

Inspired by the fact that the identity matrix correction, viz, without any correction, can be introduced to particles with ill-conditioned correction matrices, we introduce a non-linear weight between the original KGC and the identity one to automatically adjust the amount of correction by considering the matrix determinant value. To this end, the weighted KGC is rewritten

as

$$\widetilde{\mathbf{B}}_i = \frac{|\mathbf{B}_i|^\beta \mathbf{B}_i}{\alpha |\mathbf{I}| + |\mathbf{B}_i|^\beta} + \frac{\alpha \mathbf{I}}{\alpha |\mathbf{I}| + |\mathbf{B}_i|^\beta}, \quad (12)$$

here $|\cdot|$ denotes the determinant value, α and β are weighting factors, where α is a positive value and β is an integer. The weighted matrix becomes the original KGC if $\alpha = 0$. While the first term to enhance accuracy is dominant when the matrix determinant $|\mathbf{B}|$ is large, the identity matrix is dominant when $|\mathbf{B}|$ is small to avoid numerical instability. The preliminary numerical tests indicate that the values of $\alpha = 0.3$ and $\beta = 2$ are generally effective parameters.

3.2. Corrected Riemann solution

To reference the previous study [28], we only introduce the WKGC scheme into the particle-average term of the momentum equation. Therefore, it is necessary to further decompose the Riemann solution of the pressure term in Eq.(3) into the inter-particle average and dissipation terms as

$$\begin{cases} \frac{d\mathbf{v}_i}{dt} = -2 \sum_j \left(\frac{P^*}{\rho_i} \right) V_j \nabla_i W_{ij} + 2 \sum_j \frac{\nu}{\rho_i} \mathbf{v}_{ij} V_j \nabla_i W_{ij} + \mathbf{g}_i \\ P^* = p^* + \Pi^*, \end{cases} \quad (13)$$

where $p^* = \frac{\rho_{LCL} P_R + \rho_{RCR} P_L}{\rho_{LCL} + \rho_{RCR}}$ and $\Pi^* = \frac{\rho_{LCL} \rho_{RCR} (U_L - U_R) \beta}{\rho_{LCL} + \rho_{RCR}}$. To ensure momentum conservation, we implement the WKGC scheme in the particle-average pattern of Eq.(13) as

$$p^* = \frac{\rho_{LCL} P_R \mathbf{B}_i + \rho_{RCR} P_L \mathbf{B}_j}{\rho_{LCL} + \rho_{RCR}}. \quad (14)$$

3.3. Dual-criteria time stepping

As the main drawback of introducing the KGC scheme is the induced computational efforts, we adopt the dual-criterial time-stepping to increase

the computational efficiency. The dual-criterial time stepping proposed by Zhang et al.[1] consists of an advection time step and an acoustic one. The advection criterion is based on the flow velocity and controls the update frequency of the particle neighbor lists or configurations. On the other hand, the acoustic criterion is determined by the artificial speed of sound and is used for the time integration of the governing equations. Generally, the advection time step is larger than the acoustic time step, implying that several acoustic time steps are carried out in one advection time step without updating the particle configuration. Following Ref.[1], the advection and acoustic criteria are given by

$$\begin{cases} \Delta t_{ad} = 0.25 \frac{h}{|\mathbf{v}|_{max}} \\ \Delta t_{ac} = 0.6 \left(\frac{h}{c + |\mathbf{v}|_{max}} \right), \end{cases} \quad (15)$$

where h is the smoothing length, $|\mathbf{v}|_{max}$ is the maximum particle velocity.

In this study, we integrate the WKGC scheme into the dual-criterial time stepping framework. The key idea is to compute the WKGC matrix and conduct the corresponding inversion for all particles at the advection step and then we use it for several acoustic steps.

4. Numerical examples

In this part, several benchmark tests, including standing wave, oscillation drop and dam-break flow are first carried out to validate the robustness, accuracy and energy conservation properties of the proposed method. Having the validation in hand, an ocean engineering application of wave interaction i.e. OWSC [29] is simulated to investigate the versatility and performance.

The ratio of smoothing length to the particle resolution i.e. h/dp is 1.3 without specification and the corresponding cutoff radius is $2.6 dp$. It should be noted that the water pressure is zero at the initial state.

4.1. Standing wave

In this section, a 2D standing wave is computed with the initial sketch shown in Figure.1. The initial free surface is given as

$$\eta_0 = A \cos(k(x + \lambda)/2), \quad (16)$$

where the wave amplitude $A = 0.1H$, the wave number $k = 2\pi/\lambda$ and the wave length $\lambda = 2$ m. The average water depth is $H = 1.0$ m and the initial velocity of particles is zero. The free-surface elevation at the center position is measured and compared with the second-order analytical solution derived by Wu and Taylor [30] and numerical results in Ref. [31].

Figure.2 shows the time variation of the normalized mechanical energy. As expected, the present method greatly reduces the numerical dissipation compared with those without WKGC. To study the effect of the smoothing length on the energy conservation property, the time history of the normalized mechanical energy predicted by the method without the WKGC scheme under different smoothing lengths is compared with those obtained by Khayyer et al.[31] and an analytical solution, as also shown in Figure.2. It can be noted that increasing the smoothing length leads to a clear enhancement in the energy conservation properties but excessive computation efforts. More precisely, a good agreement with the analytical solution is noted for the simulation without KGC when $h = 2.0 dp$ is applied, while excessive numerical dissipation is exhibited in Ref. [31] with a similar smoothing length

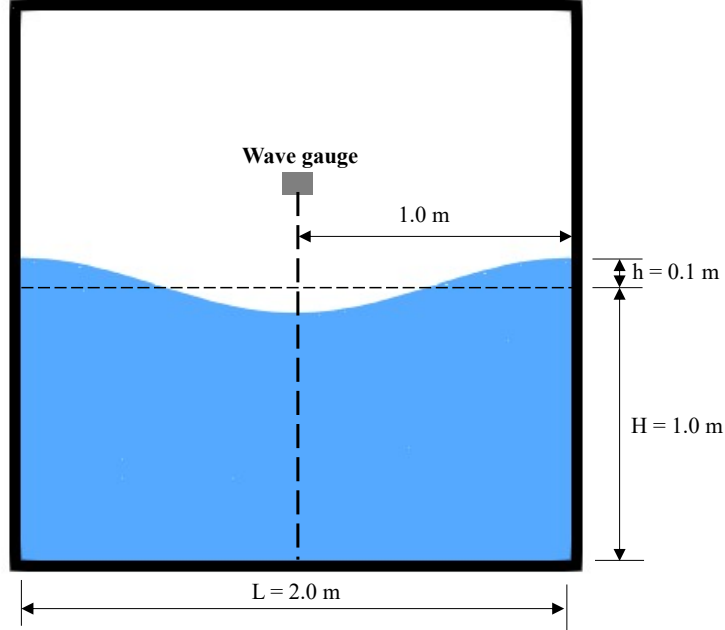


Figure 1: Standing wave: The sketch of the standing wave case.

setup.

Figure.3 (a) presents the time history of the free-surface elevation and its comparison with the analytical solution. As expected, the WKGC scheme significantly improves the numerical accuracy with fewer errors from the analytical peak and phase. Figure.3 (b) displays the convergence of the free-surface elevation with spatial resolutions. As the increase of particle resolution, convergence with the analytical solution is obtained.

Figure.4 presents predicted free-surface elevations by the method without the WKGC scheme for different smoothing lengths. Similar to the profile of mechanical energy, increasing the smoothing length provides a clear convergence with the analytical solution. To investigate the extra computational

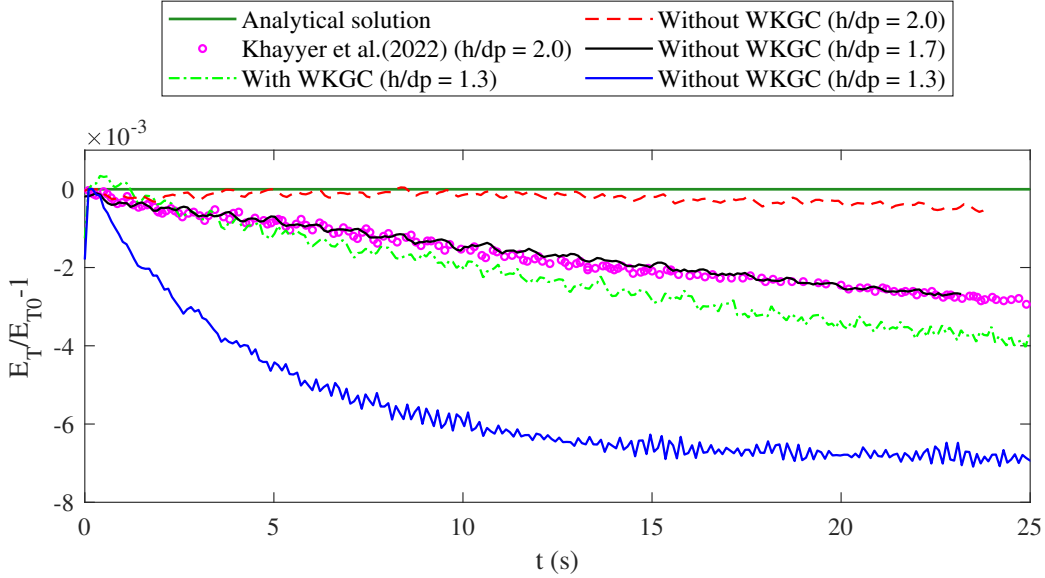


Figure 2: Standing wave: Time history of the normalized mechanical energy with different smoothing lengths. Comparison is conducted against the analytical solution and numerical results of Khayyer et al. [31] ($H/dp = 100$).

efforts induced by increasing the smoothing length, Table.2 shows the wall-clock CPU time for simulations corresponding to different smoothing lengths with and without the WKGC scheme. All the simulations are performed on a laptop with an Intel Core i7-9750H. As expected, the CPU cost increases significantly with the increase in smoothing length and the use of WKGC. Also, it is not difficult to conclude that the CPU cost increases exponentially with smoothing length for 3D simulations, as discussed in Section 4.4.

4.2. Oscillation drop

In this part, we consider an oscillating drop, which is a typical benchmark test that has been studied in the literature [14, 32, 33], to investigate the energy conservation property of the proposed method. Following Ref.[32],

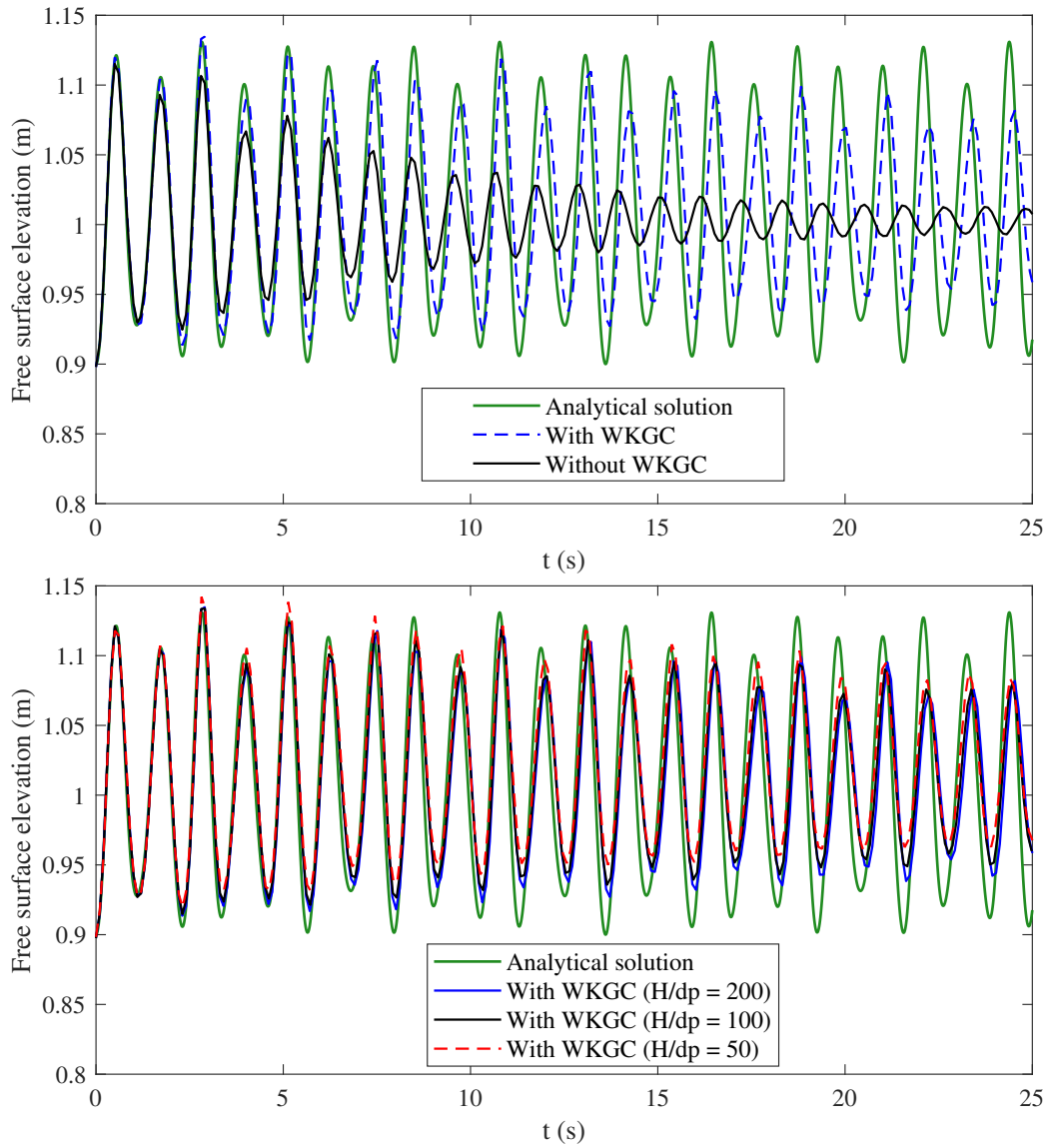


Figure 3: Standing wave: Time evolution of the free-surface elevation at the center of the tank. (a) The comparison between the method with and without the WKG scheme ($H/dp = 200$) and (b) the convergence study.

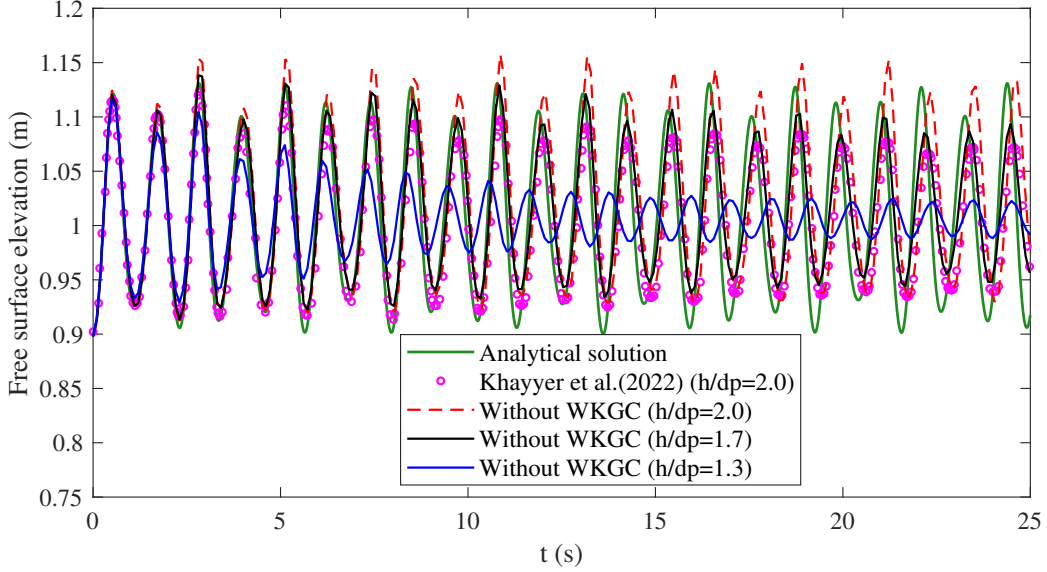


Figure 4: Standing wave: Time history of the free-surface elevation at the tank center by the method without WKGC for different smoothing lengths. Comparison is conducted against the analytical solution and numerical results of Khayyer et al.[31]($H/dp = 100$).

the drop radius is R and the fluid is considered to be inviscid. Also, the drop is under a central conservative force $f = -\Omega^2 R$ and initialized with a velocity profile

$$\begin{cases} u_0 = A_0 x \\ v_0 = -A_0 y, \end{cases} \quad (17)$$

where $A_0 = 1.0$ and $A_0/\Omega = 1.0$. Note that an analytical solution is available [34] for quantitative validation.

Figure.5 shows the free-surface profile and the pressure contour obtained by the present method at $t = 20.5$ s and $t = 22.9$ s. As expected, the present method produces a robust free-surface profile and smooth pressure field. The

Table 2: Standing wave: The CPU time with different smoothing lengths. The computations are performed on a laptop with an Intel Core i709750H CPU.

h/dp	Computing time	Physical time	Particle number	WKGC
1.3	38.43 s	1.0 s	23264	No
1.7	43.72 s	1.0 s	23264	No
2.0	46.78 s	1.0 s	23264	No
1.3	43.05 s	1.0 s	23264	Yes
1.7	48.57 s	1.0 s	23264	Yes
2.0	49.55 s	1.0 s	23264	Yes

time variation of pressure at the drop center with different particle resolutions is presented in Figure.6. A good agreement with the analytical solution is noted with increasing spatial resolutions. Figure.7 displays the time history of the semi-major axis of the drop. With the present WKGC scheme, higher numerical accuracy is achieved.

To investigate the energy conservation property, the time variation of kinetic energy and potential energy is portrayed in Figure.8. The present method presents good energy conservation characteristics and provides good consistency with the analytical solution. Figure.9 shows the time evolution of the normalized mechanical energy. Similar to Ref.[35], the mechanical energy first increases slightly and then decreases with time going. As reported by Colagrossi et al. [36] and Huang et al. [35], the initial increase of the mechanical energy is due to the particle reorder. It is also observed that the present method exhibits less numerical dissipation compared with that of Huang et al. [35]. Moreover, the mechanical energy rapidly convergences to the analytical solution as the particle resolution increases. Figure.10 shows

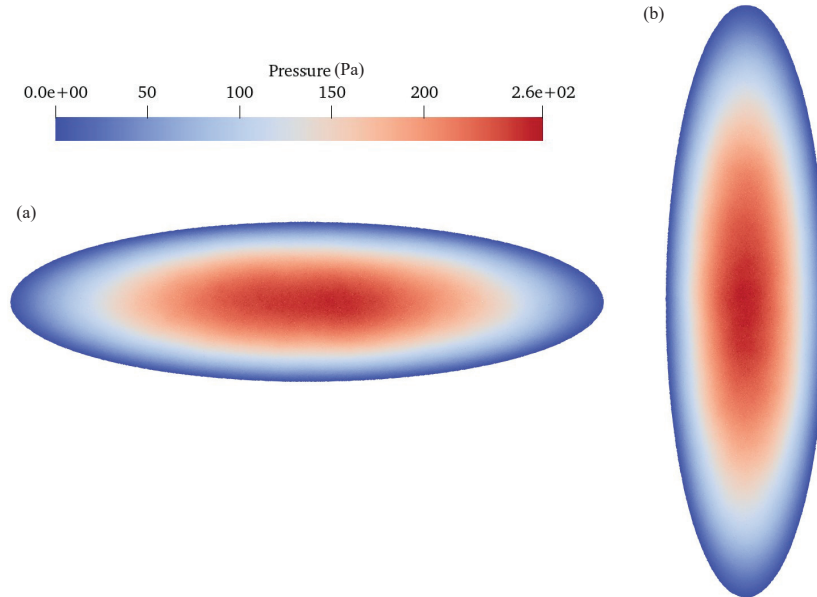


Figure 5: Oscillation drop: Snapshots of the free surface profile and the pressure contour reproduced by the present method (a) $t = 20.5$ s and (b) $t = 22.9$ s.

the time evolution of the normalized mechanical energy by the method without WKGC, Antuono et al. [32], Sun et al. [14], Hanmmmani et al. [33] with a large smoothing length $h/dp = 2.0$. Without any KGC, the method with a large smoothing length achieves better energy conservation than the methods reported in the literature [32, 14, 33].

4.3. Dam break

The dam-break flow, which has been numerically [37, 38, 13] and experimentally [39, 40, 41] investigated in the literature, is a challenging case to evaluate the stability of a SPH algorithm. The schematic is depicted in Figure.11 where four probes (E1, E2, E3 and E4) and one pressure sensor (P) are set to measure the free-surface elevation and impact pressure on the wall,

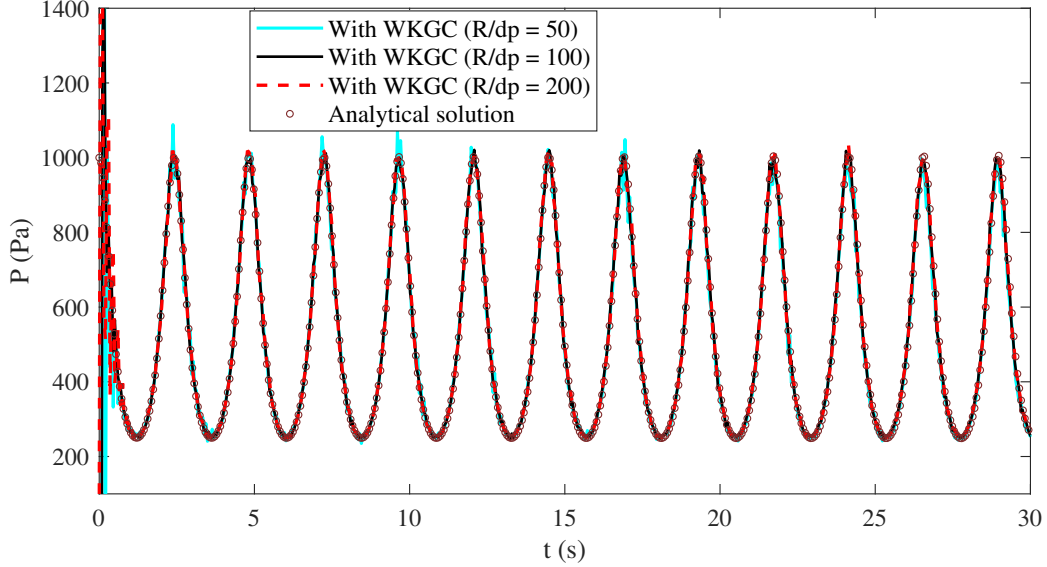


Figure 6: Oscillation drop: Time history of the pressure at the drop center with different particle resolutions.

respectively, for quantitative validation.

Figure.12 shows the snapshots of the free-surface profile and pressure contour at different time instants. The present method provides robust free-surface profiles and smooth pressure fields. The propagation wavefront predicted by the present method is compared with experimental data [39, 40, 41] and the analytical solution derived by Ritter [42] as shown in Figure.13. It can be observed that the present results agree well with experimental results [40] before $t\sqrt{g/H} < 1.0$, and are gradually close to the analytical solution at a later stage i.e. $t\sqrt{g/H} > 1.0$.

Figure.14 shows the time history of the free-surface elevation. The numerical results have good consistency with experimental data obtained by Lobovsk'y et al. [40]. Compared with the experimental data reported by

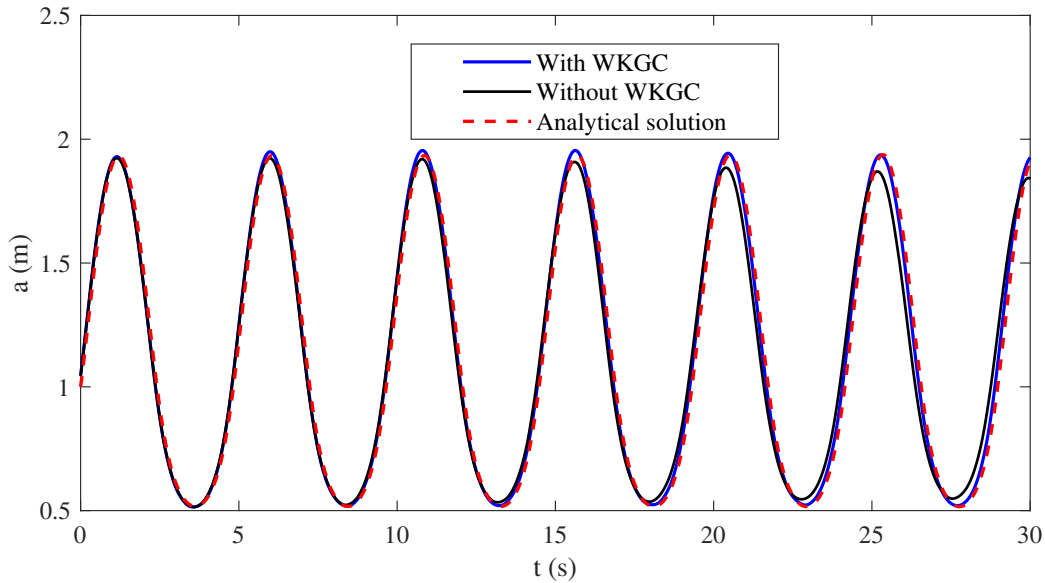


Figure 7: Oscillation drop: Time variation of the semi-major axis of the drop predicted by the method with and without the WKGC scheme ($R/dp = 50$).

Buchner [39], the present dam break waves propagate faster similar to the observation of Lobovsk'y et al. [40], leading to higher-up waves. Lobovsk'y et al. [40] pointed out that this may be due to the fact that the bed downstream in his experiment was completely dry, while not in the experiment of Buchner [39]. It should be noted that there are some discrepancies in the arrival time and the following evolution of the secondary wave [40] between the numerical results and experimental observation. This is mainly due to the fact that the secondary wave accompanies the wave breaking and re-entry. The time history of the pressure probed at P is presented in Fig.15. The numerical results are consistent with previous simulations reported in Refs [13, 37] and are in reasonable agreement with experimental data, except for the pressure oscillation resulting from the weakly compressible assumption.

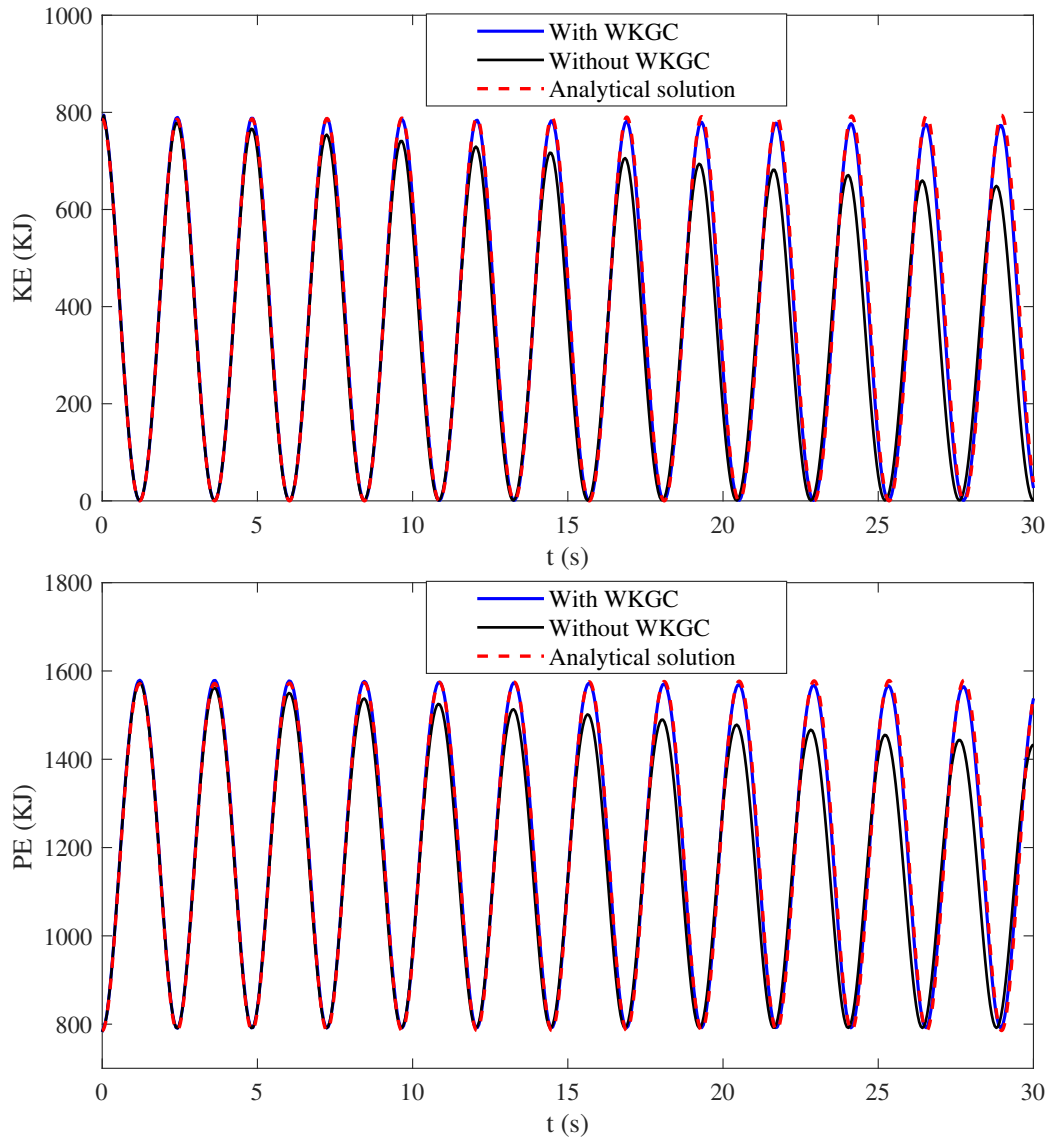


Figure 8: Oscillation drop: Time history of the kinetic energy (a) and potential energy(b) by the method with and without the WKGC scheme ($R/dp = 50$).

Figure.16 displays the mechanical energy evolution and its comparison against numerical results in the literature [13, 42]. Following Refs.[15, 13],

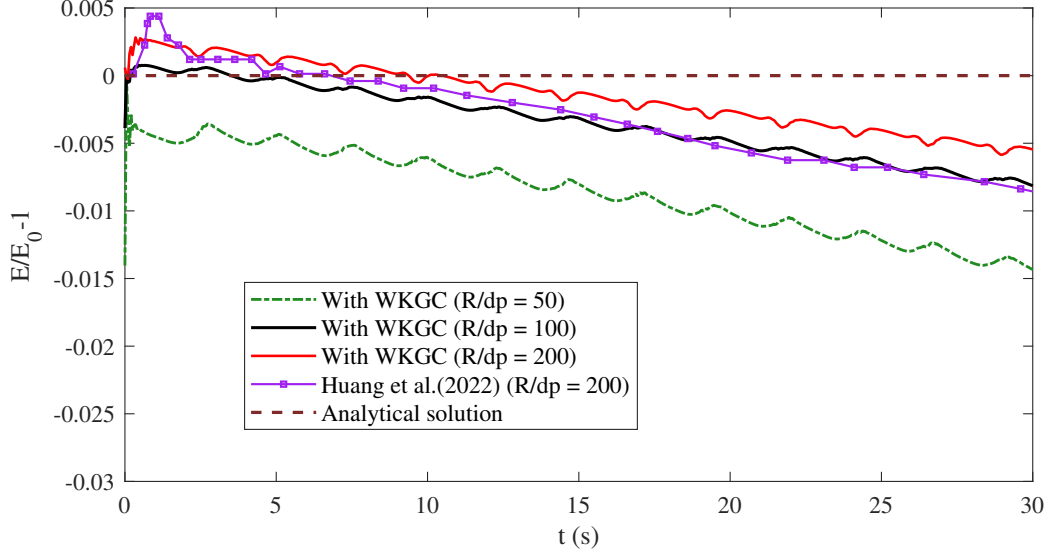


Figure 9: Oscillation drop: Time evolution of the normalized mechanical energy by the present method with different particle resolutions, Huang et al.[35] and the analytical solution.

the mechanical energy is normalized $(E - E_0)/(E_0 - E_\infty)$, where E the mechanical energy, E_0 the initial mechanical energy and E_∞ the mechanical energy after reaching the equilibrium state. As the particle resolution increases, the numerical dissipation rapidly decreases as shown in Figure.16 (a), indicating the convergence of the present method. Figure.16 (b) shows that the present method outperforms the method without WKGC in terms of energy conservation property. Also, the present method exhibits considerably less numerical dissipation compared with the results in the literature.

4.4. OWSC

In this section, we apply the present WKGC scheme to study wave interaction with an oscillating wave surge converter (OWSC) which has been

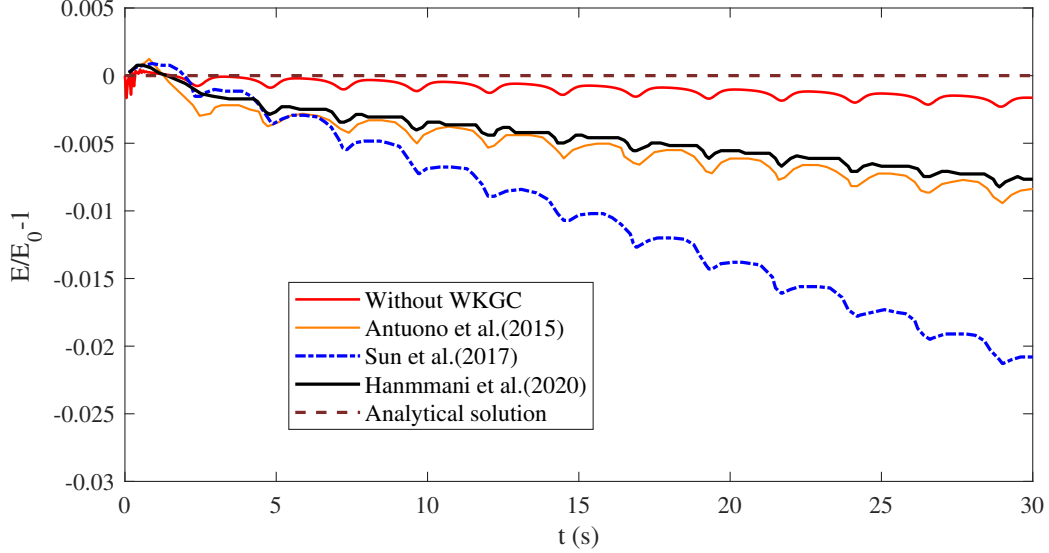


Figure 10: Oscillation drop: Time evolution of the normalized mechanical energy reproduced by the method without the WKGC scheme, Antuono et al.[32], Sun et al.[14], Hanmmami et al.[33] and the analytical solution [34] ($R/dp = 200$ and $h/dp = 2.0$).

recognized as a promising wave energy converter (WEC) and numerically and experimentally studied in the literature [43, 44, 45]. In this work, both 2D and 3D simulations are conducted. The schematic is shown in Figure.17 where the wave tank dimension is 18.2 (length) \times 4.58 (width) \times 1.0 (height) m^3 with 1:25 scale [45]. The OWSC device is simplified as a flap with a height of 0.48 m, a width of 1.04 m and a thickness of 0.12 m, hinged to a 0.16 m high base. The mass of the flap is 33 kg and its angular inertia is 1.84 kg/m^2 . For the coupling of the fluid solver and the rigid-body dynamics, we refer to Ref.[45] for more details. To discretize the system, the particle resolution is 0.03 m resulting in 13104 particles and 2.19 million particles for the 2D and 3D discretization, respectively. Three wave gauges and six pressure sensors

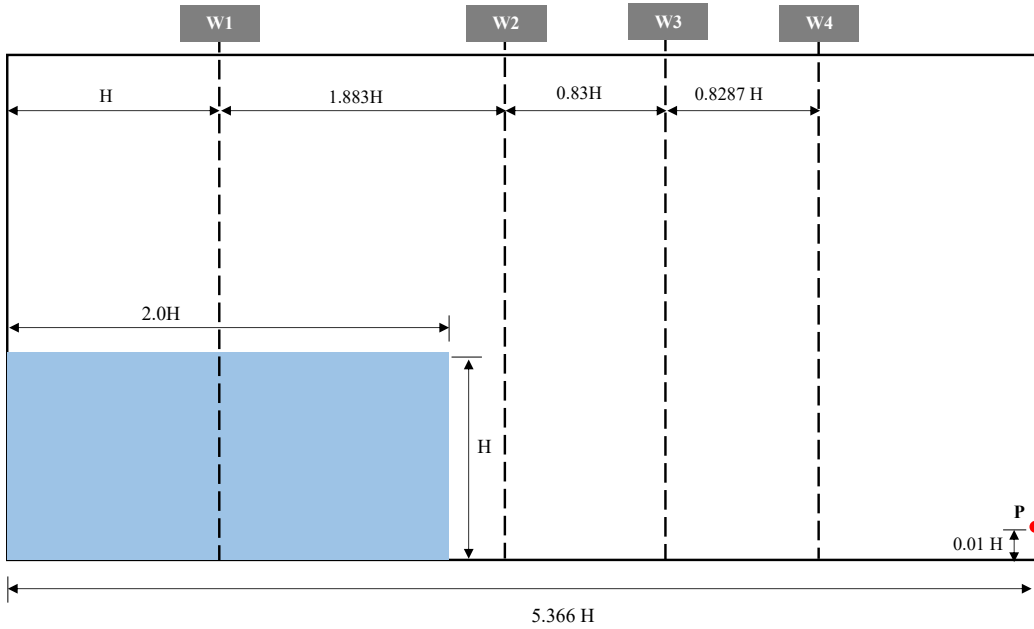


Figure 11: Dam-break: The sketch of the initial condition.

are applied to measure the wave elevation and impact pressure on the flap as shown in Figure.17. The positions of pressure sensors are presented in Table 3.

Table 3: OWSC: Positions of the pressure sensors on the front flap face. The position along the z -axis is measured from the center of the device, and $y = 0$ denotes the mean water level.

No.	y -axis (m)	z -axis (m)	No.	y -axis (m)	z -axis (m)
PS01	-0.046	0.468	PS09	-0.117	0.156
PS03	0.050	0.364	PS11	0.025	0.052
PS05	-0.300	0.364	PS13	-0.239	0.052

For the wave making, we apply the piston-type wave maker to generate

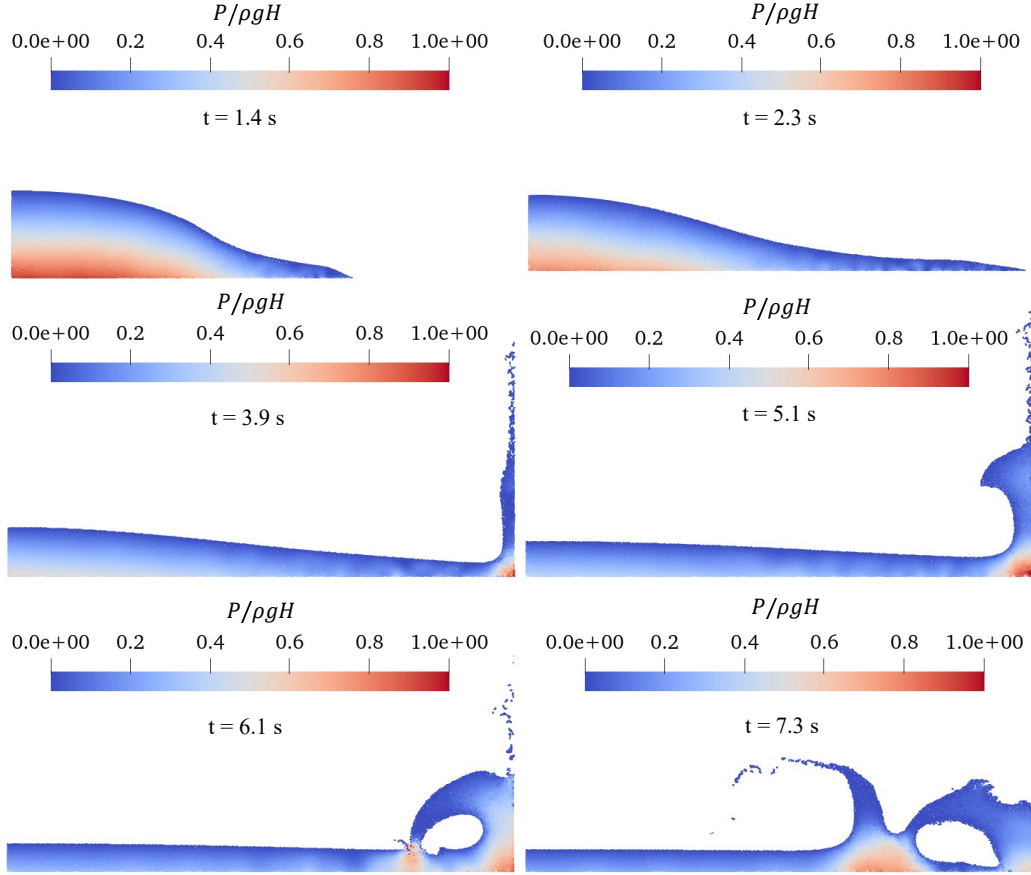


Figure 12: Dam-break: Snapshots of the free-surface profile and pressure contour reproduced by present method at different time instants.

the regular wave where the displacement of the wave maker is obtained from linear wavemaker theory [46]

$$\mathbf{r} = \frac{1}{2}S\sin(ft + \phi), \quad (18)$$

where S is the wave stroke, f the wave frequency and ϕ the initial phase.

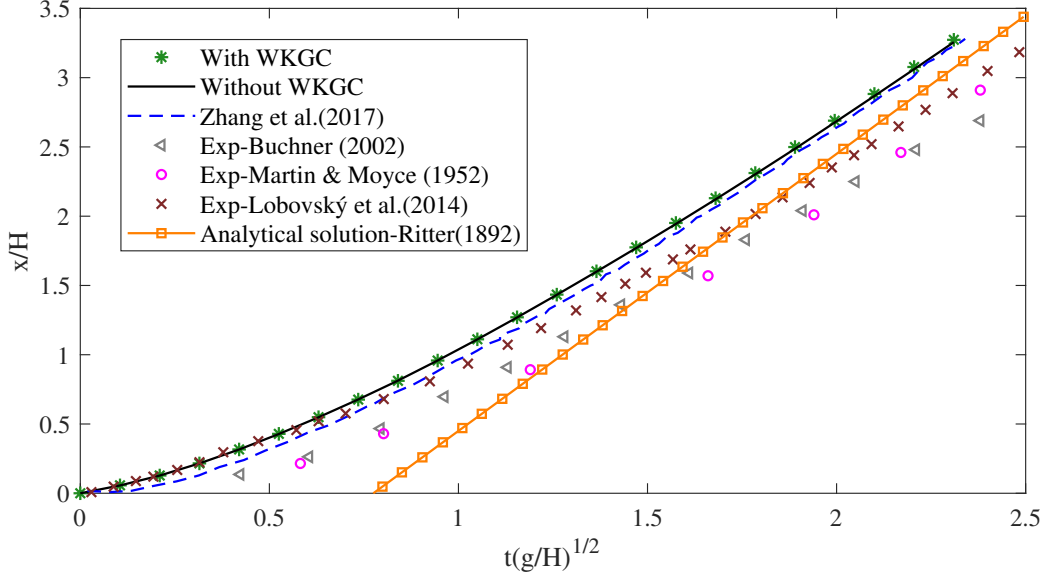


Figure 13: Dam-break: Time variation of the wavefront ($H/dp = 100$).

Also the wave stroke is given by

$$S = \frac{0.5Hkg/\omega^2}{\sinh(kh_0)\cosh(kh_0)} (\sinh(2kh_0) + 2kh_0), \quad (19)$$

where H is the wave height, k the wave number ($k = 2\pi/\lambda$) and h_0 the water depth. To avoid the effect of wave reflection, a damping zone [47] is set at the end of the tank where the particle velocity decays as

$$\mathbf{v} = \mathbf{v}_0 \left(1.0 - \alpha \Delta t \left(\frac{\mathbf{r} - \mathbf{r}_{a0}}{\mathbf{r}_{ae} - \mathbf{r}_{a0}} \right) \right), \quad (20)$$

where \mathbf{v}_0 is the velocity of fluid particles at the entry of the sponge layer, $\alpha = 5.0$ the damping coefficient, \mathbf{r}_{a0} and \mathbf{r}_{ae} are the beginning and end position of the sponge layer, respectively.

Figure.18 presents snapshots of the free-surface profile colored by velocity magnitude. It can be noted that the present method can capture the violent

free-surface elevation involving impacting break and re-entry, and produce a smooth velocity field. The cutting slice along the center of the wave tank portrays the wave reflection and breaking around the flap.

Figure.19 shows the time history of the wave elevation. The present results exhibit an improvement compared to the results obtained without the KGC scheme and demonstrate reasonable agreement with the experimental data. While some discrepancies in wave crest and phase are noted. One possible reason is that wave reflection and breaking occur around the flap, as also shown in Figure.18. Another reason could be attributed to the absence of a turbulence model, which may strongly affect the interaction between wave and flap. The overestimate of wave crests is due to the less dissipation after utilizing the WKGC scheme. While Wei et al.[44] adopted the standard $k-\varepsilon$ turbulence model, which introduces more dissipation to the simulation.

Figure.20 presents the time history of the rotation of the flap obtained by the present method and the method without WKGC, and its comparison with other published numerical results [43, 44] and experimental data [44]. The present numerical results show clear improvements and agree better with the experimental data compared with that without WKGC. Compared with the results obtained by Wei et al.[44], the SPH predictions generally underestimated rotation due to the lack of a turbulence model. Compared with SPH results in Refs. [43, 45], the WKGC scheme can predict flap motion more accurately with less deviation from the experimental rotation crest.

Figure.21 presents the time history of the probed pressure on the flap obtained by the present method and its comparison with that of Wei et al. [44] and experimental data [44]. Generally, the results show good agreement.

For pressure sensors PS01, PS03, PS09 and PS11, the slamming pressure can be well captured except for some high-frequency pressure oscillations. Compared to Wei’s numerical results, the present method effectively captures the double peak and agrees better with experimental data. Similar to the numerical results from Wei et al. [44], the pressure drops of the present method are underestimated compared with the experimental observation for sensors PS05 and PS13. This difference originates mainly from the weakly compressible assumption in the present method and the splash passing the flap usually accompanies the air entrainment which is not considered in the numerical model.

The computational efficiency of the present method with and without WKGC is analyzed in Table 4. The 3D simulations are carried out on an Intel(R) Xeon(R) Platinum 9242 CPU @ 2.30GHz with 48 cores and the 2D ones are on an Intel Core i7-9750H laptop with 6 cores. For the 3D simulations, the introduction of the present WKGC slightly increases the computational wall clock time while the induced extra computational efforts are negligible for 2D simulations.

5. Conclusions

In this paper, we proposed an efficient, robust and simple WKGC scheme to address the issue of numerical instability and computational efficiency for introducing the KGC scheme in the Riemann-SPH method. The underlying principle is to introduce a weighted value of the original KGC matrix and the identity one, implement it in a particle-average manner and cooperate it into a dual-criteria time stepping framework. Extensive examples, including

standing wave, oscillating drop, dam-break flow and wave interacting with an OWSC, are investigated to demonstrate that the present WKGC scheme can stably resolve violent free surface flows, reproduce a smooth pressure field, reduce numerical dissipation meanwhile induces limited extra computational efforts.

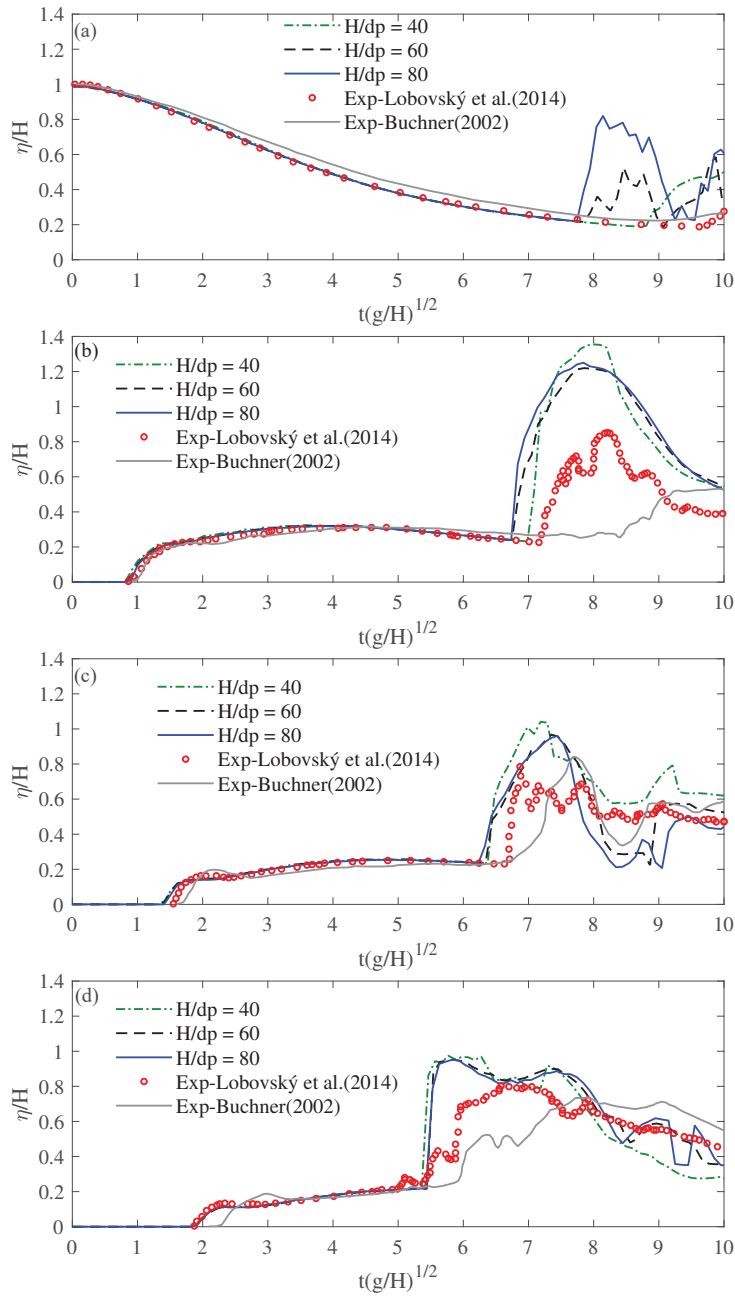


Figure 14: Dam-break: Time history of free-surface elevation at wave gauges W1 (a), W2 (b), W3 (c) and W4 (d).

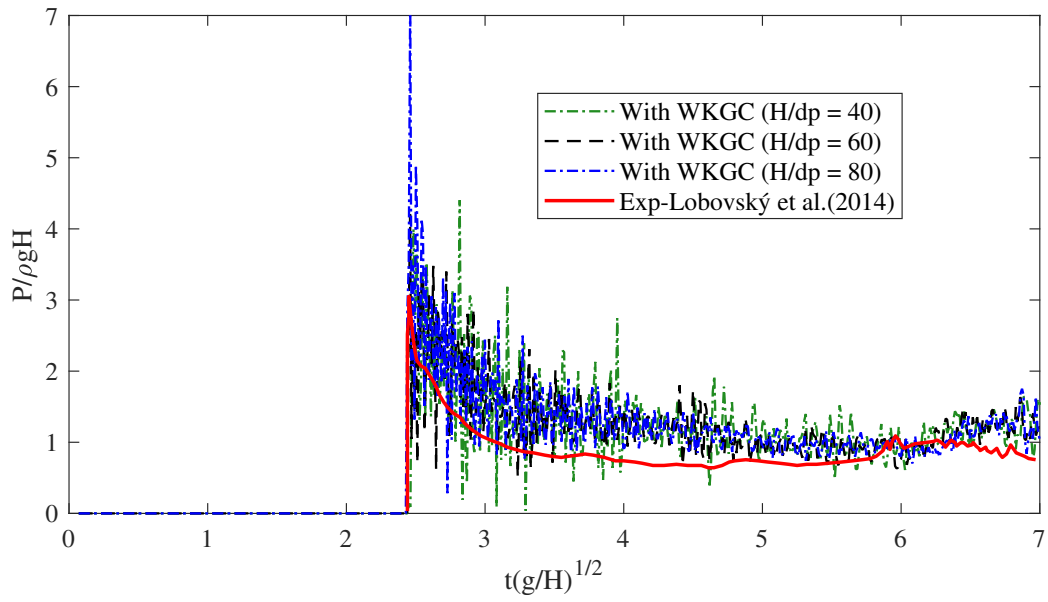


Figure 15: Dam-break: Time variation of the pressure probed at P.

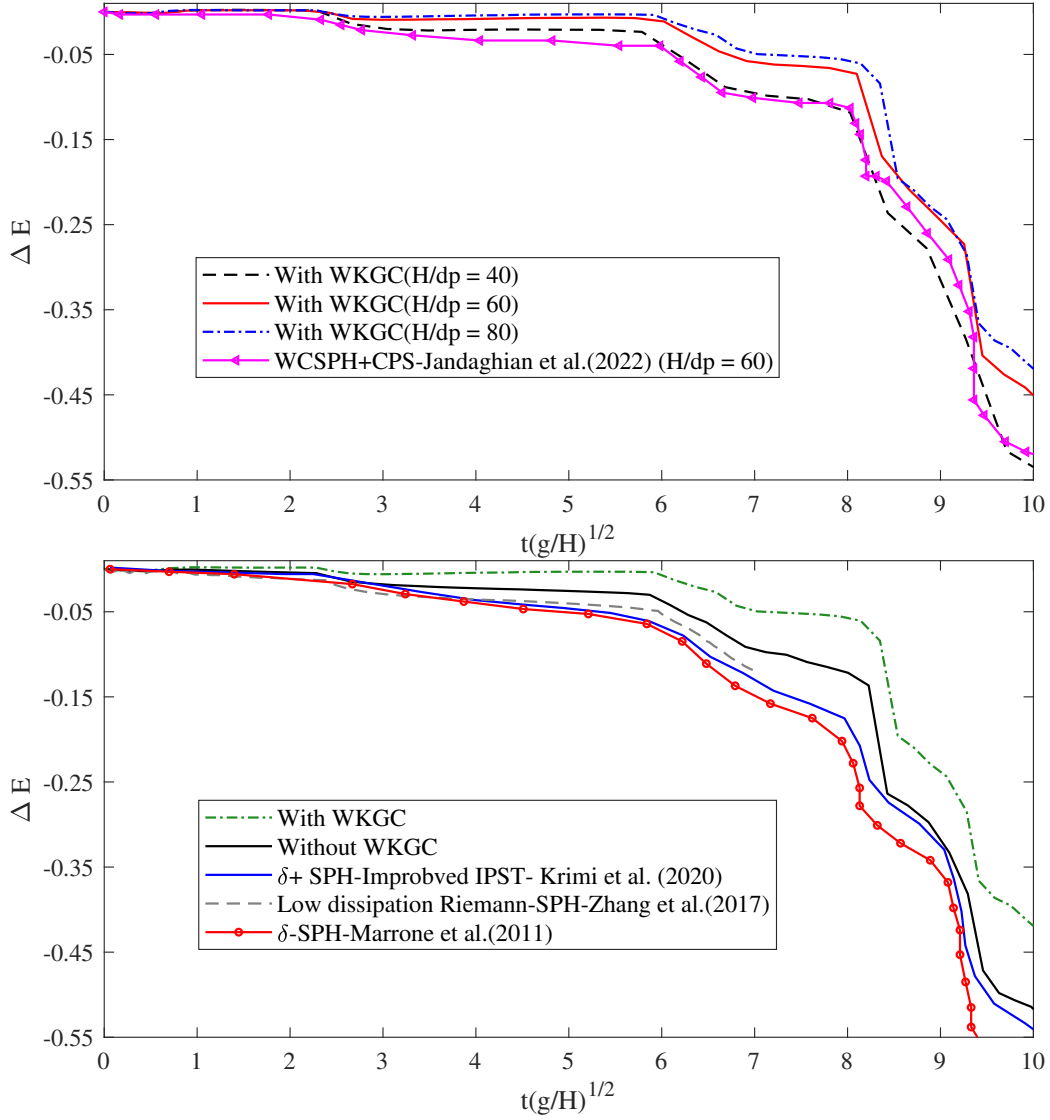


Figure 16: Dam-break: Time evolution of the mechanical energy. Convergence study of the present method (a) and the comparison with other numerical results in the literature ($H/dp = 80$)(b).

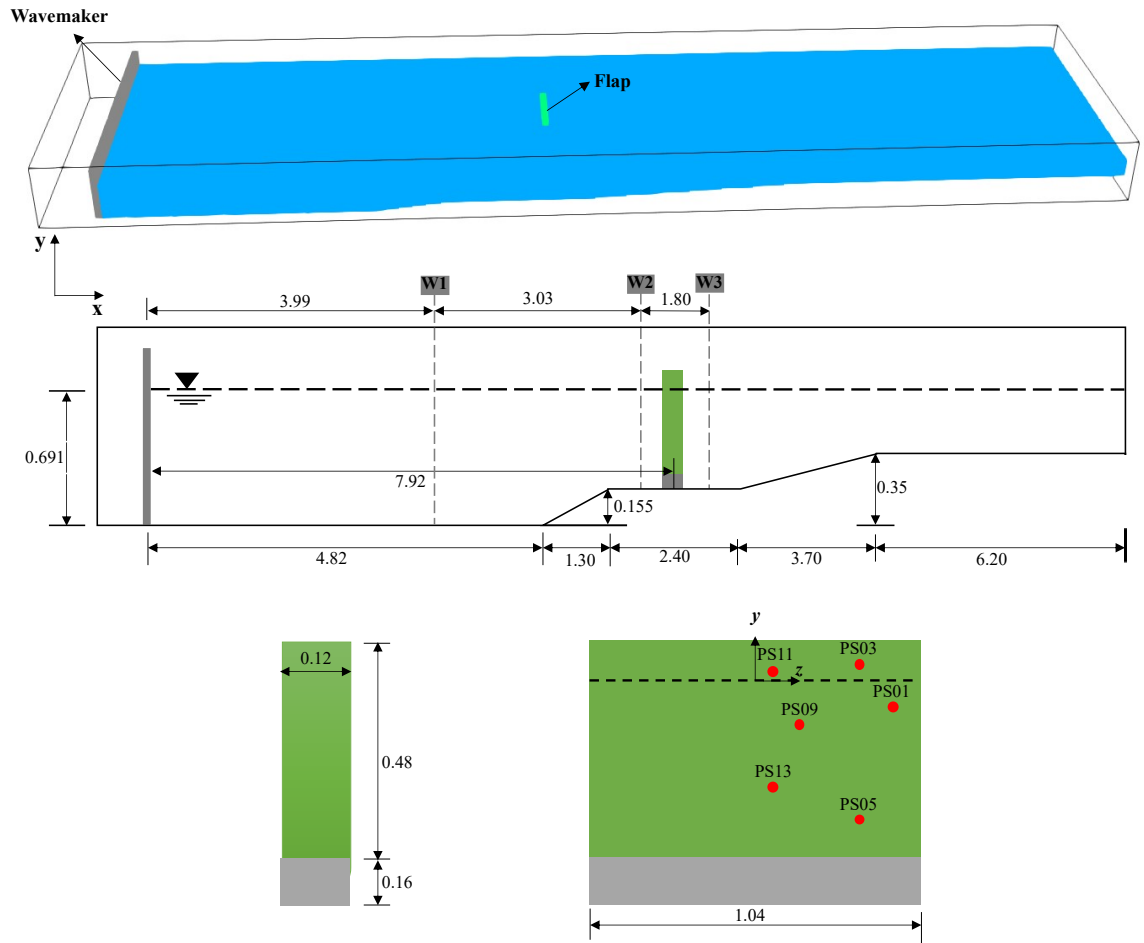


Figure 17: OWSC: The initial sketch.

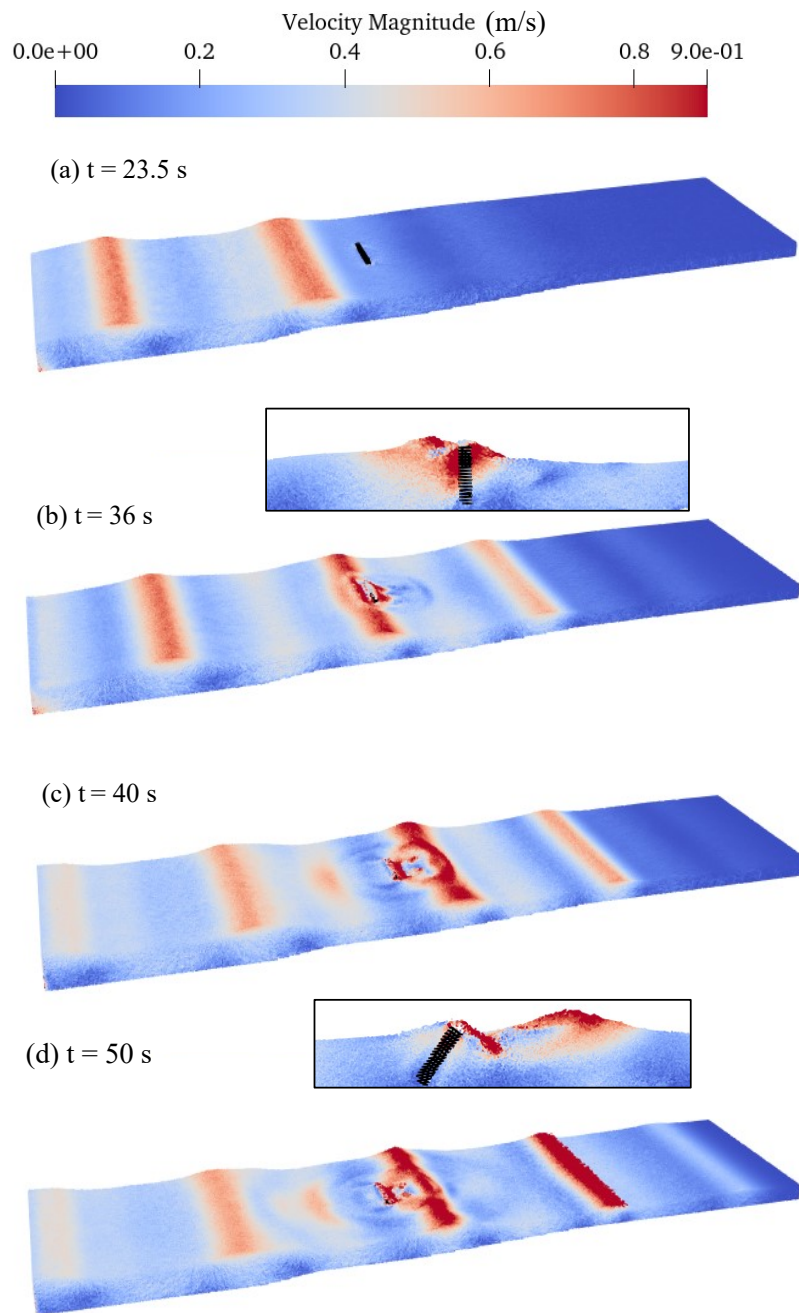


Figure 18: OWSC: Snapshots of the free-surface profile colored by velocity magnitude.

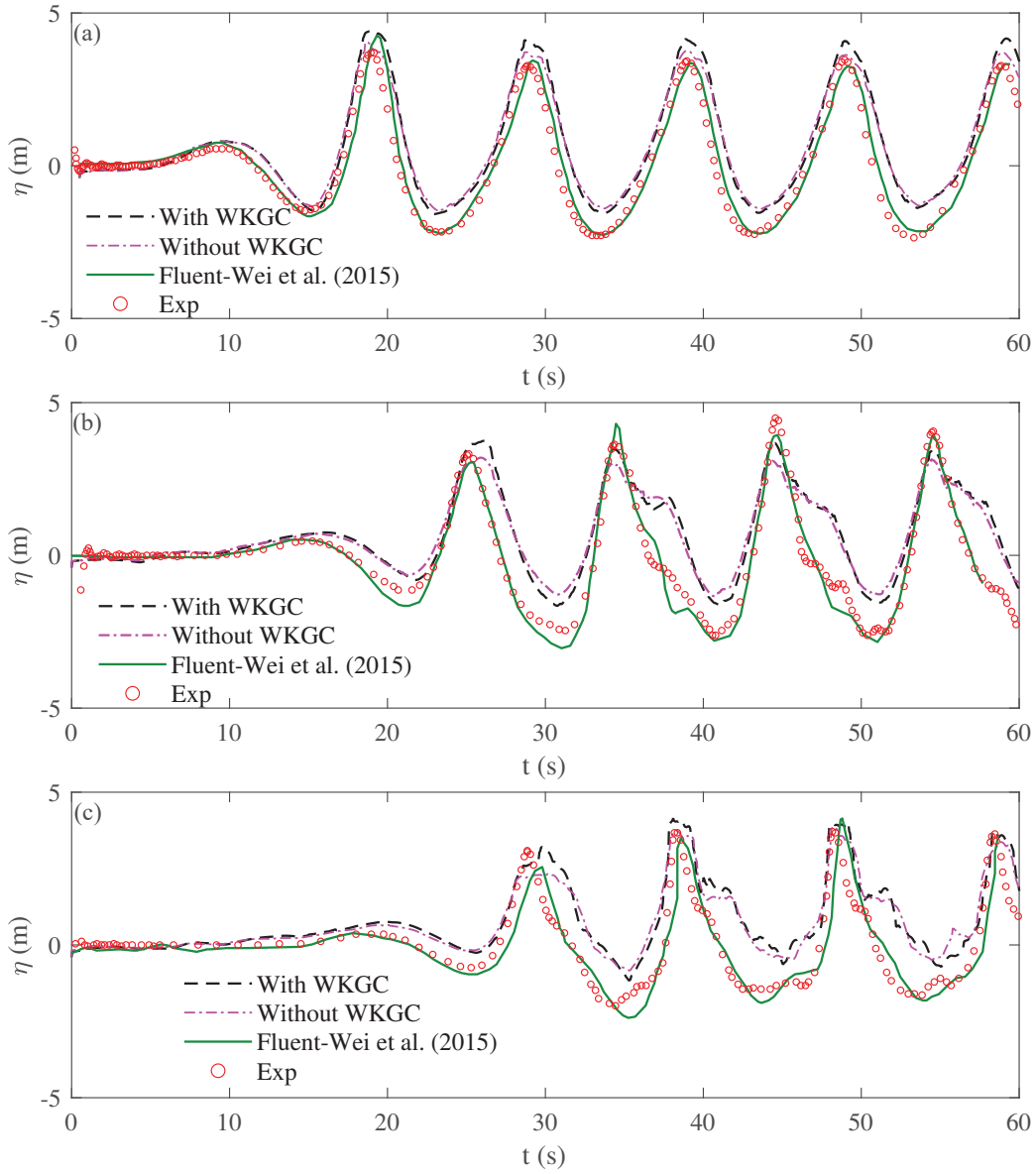


Figure 19: OWSC: Time history of the free-surface elevation at W1(a), W2(b) and W3(c).

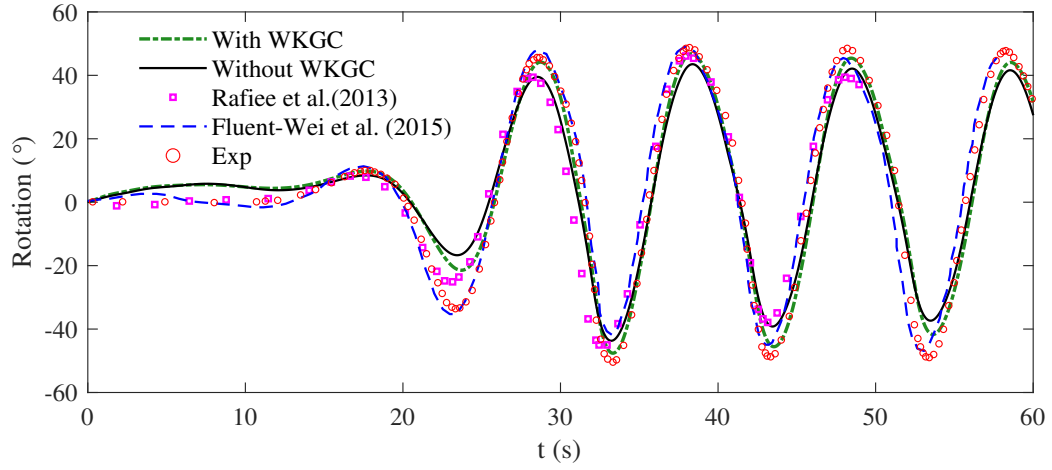


Figure 20: OWSC: Time evolution of the flap rotation.

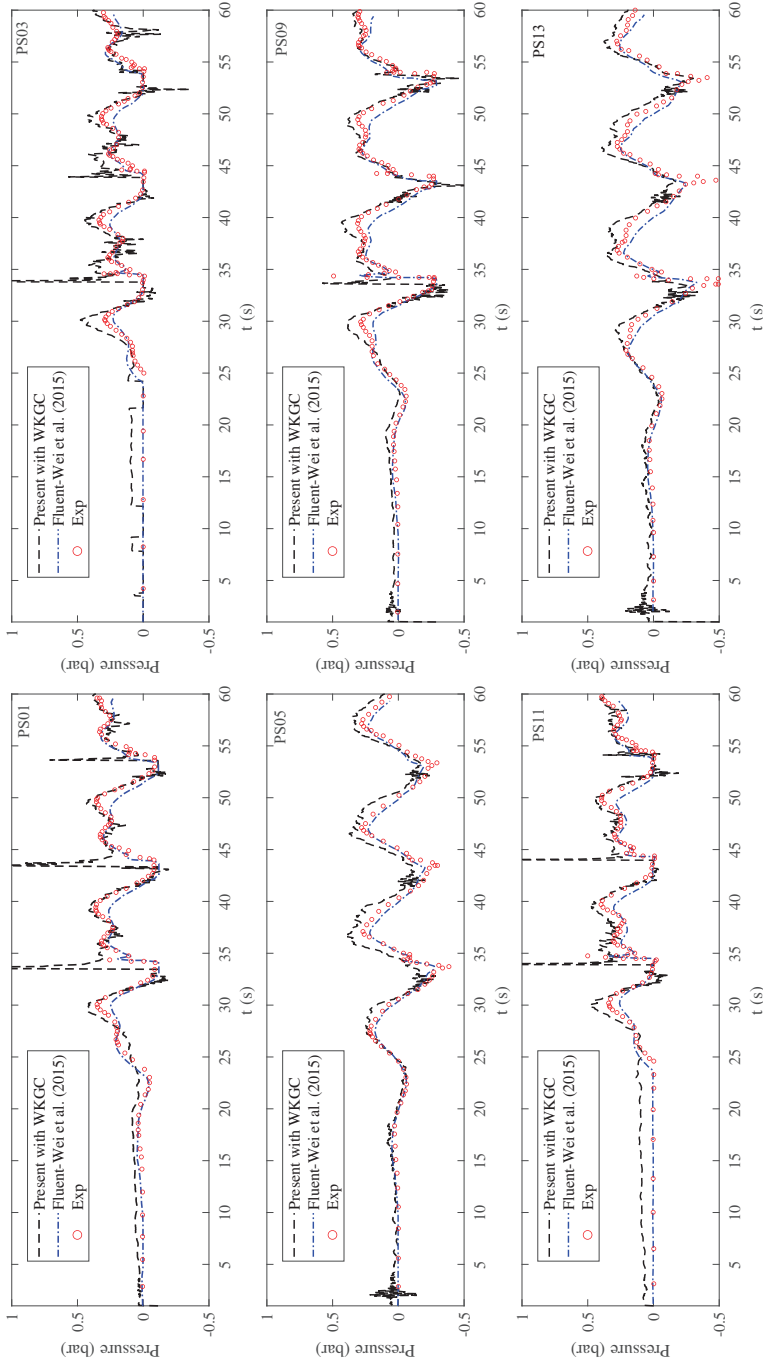


Figure 21: OWSC: Time history of pressure on the flap obtained by the present method and its comparison with that of Wei et al.[44].

Table 4: OWSC: The CPU wall-clock time for both 2D and 3D simulations.

Model	Computational time	Physical time	Particle number	Device Info
With WKGC (3D)	4.58 h	13.8 s	2.19 million	48 cores Intel Xeon Platinum 9242
Without WKGC (3D)	3.97 h	13.8 s	2.19 million	48 cores Intel Xeon Platinum 9242
With WKGC (2D)	165.06 s	13.8 s	13104	6 cores Intel Core i7-9750H
Without WKGC (2D)	153.78 s	13.8 s	13104	6 cores Intel Core i7-9750H

CRediT authorship contribution statement

Yaru Ren: Investigation, Methodology, Visualization, Formal analysis, Writing - original draft, Writing - review & editing; **Pengzhi Lin:** Investigation, Supervision, Writing - review & editing; **Chi Zhang:** Investigation, Methodology, Formal analysis, Writing - review & editing; **Xiangyu Hu:** Investigation, Supervision, Writing - review & editing.

Declaration of competing interest

The authors declare that they have no known competing financial interests or personal relationships that could have appeared to influence the work reported in this paper.

6. Acknowledgement

C. Zhang and X.Y. Hu would like to express their gratitude to Deutsche Forschungsgemeinschaft (DFG) for their sponsorship of this research under grant numbers HU1527/12-4.

References

- [1] C. Zhang, M. Rezavand, X. Hu, Dual-criteria time stepping for weakly compressible smoothed particle hydrodynamics, *Journal of Computational Physics* 404 (2020) 109135.
- [2] H. Gotoh, A. Khayyer, On the state-of-the-art of particle methods for coastal and ocean engineering, *Coastal Engineering Journal* 60 (1) (2018) 79–103.
- [3] M. Luo, A. Khayyer, P. Lin, Particle methods in ocean and coastal engineering, *Applied Ocean Research* 114 (2021) 102734.
- [4] C. Zhang, Y.-j. Zhu, D. Wu, N. A. Adams, X. Hu, Smoothed particle hydrodynamics: Methodology development and recent achievement, *Journal of Hydrodynamics* 34 (5) (2022) 767–805.
- [5] D. Violeau, B. D. Rogers, Smoothed particle hydrodynamics (sph) for free-surface flows: past, present and future, *Journal of Hydraulic Research* 54 (1) (2016) 1–26.
- [6] C. Altomare, A. J. Crespo, J. M. Domínguez, M. Gómez-Gesteira, T. Suzuki, T. Verwaest, Applicability of smoothed particle hydrody-

- namics for estimation of sea wave impact on coastal structures, *Coastal Engineering* 96 (2015) 1–12.
- [7] V. Springel, Smoothed particle hydrodynamics in astrophysics, *Annual Review of Astronomy and Astrophysics* 48 (2010) 391–430.
- [8] J. Wang, D. Chan, Frictional contact algorithms in sph for the simulation of soil–structure interaction, *International Journal for Numerical and Analytical Methods in Geomechanics* 38 (7) (2014) 747–770.
- [9] P. Guilcher, G. Ducorzet, B. Alessandrini, P. Ferrant, Water wave propagation using sph models, in: *Proceedings 2 nd International Spheric Workshop*, 2007, pp. 119–122.
- [10] T. Kanehira, M. L. McAllister, S. Draycott, T. Nakashima, D. M. Ingram, T. S. van den Bremer, H. Mutsuda, The effects of smoothing length on the onset of wave breaking in smoothed particle hydrodynamics (sph) simulations of highly directionally spread waves, *Computational Particle Mechanics* (2022) 1–17.
- [11] A. Khayyer, H. Gotoh, Y. Shimizu, K. Gotoh, On enhancement of energy conservation properties of projection-based particle methods, *European Journal of Mechanics-B/Fluids* 66 (2017) 20–37.
- [12] V. Zago, L. J. Schulze, G. Bilotta, N. Almashan, R. Dalrymple, Overcoming excessive numerical dissipation in sph modeling of water waves, *Coastal Engineering* 170 (2021) 104018.
- [13] S. Marrone, M. Antuono, A. Colagrossi, G. Colicchio, D. Le Touzé,

- G. Graziani, δ -sph model for simulating violent impact flows, *Computer Methods in Applied Mechanics and Engineering* 200 (13-16) (2011) 1526–1542.
- [14] P. Sun, A. Colagrossi, S. Marrone, A. Zhang, The δ plus-sph model: Simple procedures for a further improvement of the sph scheme, *Computer Methods in Applied Mechanics and Engineering* 315 (2017) 25–49.
- [15] C. Zhang, X. Hu, N. A. Adams, A weakly compressible sph method based on a low-dissipation riemann solver, *Journal of Computational Physics* 335 (2017) 605–620.
- [16] Y. Ren, P. Lin, A. Khayyer, M. Luo, Comparative analysis of three smoothed particle hydrodynamics methods in modeling free-surface flows, *International Journal of Offshore and Polar Engineering* 32 (03) (2022) 267–274.
- [17] A. Colagrossi, A. Souto-Iglesias, M. Antuono, S. Marrone, Smoothed-particle-hydrodynamics modeling of dissipation mechanisms in gravity waves, *Physical Review E* 87 (2) (2013) 023302.
- [18] P. Randles, L. D. Libersky, Smoothed particle hydrodynamics: some recent improvements and applications, *Computer methods in applied mechanics and engineering* 139 (1-4) (1996) 375–408.
- [19] J. Bonet, T.-S. Lok, Variational and momentum preservation aspects of smooth particle hydrodynamic formulations, *Computer Methods in applied mechanics and engineering* 180 (1-2) (1999) 97–115.

- [20] A. Khayyer, H. Gotoh, S. Shao, Corrected incompressible sph method for accurate water-surface tracking in breaking waves, *Coastal Engineering* 55 (3) (2008) 236–250.
- [21] H. Wen, B. Ren, X. Yu, An improved sph model for turbulent hydrodynamics of a 2d oscillating water chamber, *Ocean Engineering* 150 (2018) 152–166.
- [22] Y. Xiao, X. Hong, Z. Tang, Normalized sph without boundary deficiency and its application to transient solid mechanics problems, *Meccanica* 55 (11) (2020) 2263–2283.
- [23] J. P. Vila, Sph renormalized hybrid methods for conservation laws: applications to free surface flows, in: *Meshfree methods for partial differential equations II*, 2005, pp. 207–229.
- [24] S. L. Z. V., B. G., D. R.A., Localized kernel gradient correction for sph simulations of water wave propagation, *Proceedings of the 16th SPHERIC International Workshop* (2022).
- [25] Z. Zhang, M. Liu, A decoupled finite particle method for modeling incompressible flows with free surfaces, *Applied Mathematical Modelling* 60 (2018) 606–633.
- [26] J. J. Monaghan, Smoothed particle hydrodynamics, *Annual review of astronomy and astrophysics* 30 (1992) 543–574.
- [27] T. Ye, D. Pan, C. Huang, M. Liu, Smoothed particle hydrodynamics (sph) for complex fluid flows: Recent developments in methodology and applications, *Physics of Fluids* 31 (1) (2019) 011301.

- [28] H. Xiaoting, S. Pengnan, L. Hongguan, Z. Shiyun, Development of a numerical wave tank with a corrected smoothed particle hydrodynamics scheme to reduce nonphysical energy dissipation, *Chinese Journal of Theoretical and Applied Mechanics* 54 (6) (2022) 1502–1515.
- [29] T. Whittaker, D. Collier, M. Folley, M. Osterried, A. Henry, M. Crowley, The development of oyster—a shallow water surging wave energy converter, in: *Proceedings of the 7th European wave and tidal energy conference, 2007*, pp. 11–14.
- [30] G. Wu, R. E. Taylor, Finite element analysis of two-dimensional nonlinear transient water waves, *Applied Ocean Research* 16 (6) (1994) 363–372.
- [31] A. Khayyer, Y. Shimizu, T. Gotoh, H. Gotoh, Enhanced resolution of the continuity equation in explicit weakly compressible sph simulations of incompressible free-surface fluid flows, *Applied Mathematical Modelling* (2022).
- [32] M. Antuono, S. Marrone, A. Colagrossi, B. Bouscasse, Energy balance in the δ -sph scheme, *Computer Methods in Applied Mechanics and Engineering* 289 (2015) 209–226.
- [33] I. Hammani, S. Marrone, A. Colagrossi, G. Oger, D. Le Touzé, Detailed study on the extension of the δ -sph model to multi-phase flow, *Computer Methods in Applied Mechanics and Engineering* 368 (2020) 113189.
- [34] J. J. Monaghan, A. Rafiee, A simple sph algorithm for multi-fluid flow

- with high density ratios, *International Journal for Numerical Methods in Fluids* 71 (5) (2013) 537–561.
- [35] H. Xiaoting, S. Pengnan, L. Hongguan, Z. Shiyun, Development of a numerical wave tank with a corrected smoothed particle hydrodynamics scheme to reduce nonphysical energy dissipation, *Chinese Journal of Theoretical and Applied Mechanics* 54 (6) (2022) 1502–1515.
- [36] A. Colagrossi, B. Bouscasse, M. Antuono, S. Marrone, Particle packing algorithm for sph schemes, *Computer Physics Communications* 183 (8) (2012) 1641–1653.
- [37] M. Jandaghian, H. M. Siaben, A. Shakibaeinia, Stability and accuracy of the weakly compressible sph with particle regularization techniques, *European Journal of Mechanics-B/Fluids* 94 (2022) 314–333.
- [38] A. Krimi, M. Jandaghian, A. Shakibaeinia, A wcsph particle shifting strategy for simulating violent free surface flows, *Water* 12 (11) (2020) 3189.
- [39] B. Buchner, Green water on ship-type offshore structures, Ph.D. thesis, Delft University of Technology Delft, The Netherlands (2002).
- [40] L. Lobovský, E. Botia-Vera, F. Castellana, J. Mas-Soler, A. Souto-Iglesias, Experimental investigation of dynamic pressure loads during dam break, *Journal of Fluids and Structures* 48 (2014) 407–434.
- [41] J. Martin, W. Moyce, J. Martin, W. Moyce, W. G. Penney, A. Price, C. Thornhill, Part v. an experimental study of the collapse of fluid

- columns on a rigid horizontal plane, *Philosophical Transactions of the Royal Society of London. Series A, Mathematical and Physical Sciences* 244 (882) (1952) 325–334.
- [42] R. A, Die fortpflanzung de wasserwellen, *Zeitschrift Verein Deutscher Ingenieure* 36 (33) (1892) 947–954.
- [43] A. Rafiee, B. Elsaesser, F. Dias, Numerical simulation of wave interaction with an oscillating wave surge converter, in: *International Conference on Offshore Mechanics and Arctic Engineering*, Vol. 55393, American Society of Mechanical Engineers, 2013, p. V005T06A013.
- [44] Y. Wei, A. Rafiee, A. Henry, F. Dias, Wave interaction with an oscillating wave surge converter, part i: Viscous effects, *Ocean Engineering* 104 (2015) 185–203.
- [45] C. Zhang, Y. Wei, F. Dias, X. Hu, An efficient fully lagrangian solver for modeling wave interaction with oscillating wave surge converter, *Ocean Engineering* 236 (2021) 109540.
- [46] R. G. Dean, R. A. Dalrymple, *Water wave mechanics for engineers and scientists*, Vol. 2, world scientific publishing company, 1991.
- [47] S. J. Lind, R. Xu, P. K. Stansby, B. D. Rogers, Incompressible smoothed particle hydrodynamics for free-surface flows: A generalised diffusion-based algorithm for stability and validations for impulsive flows and propagating waves, *Journal of Computational Physics* 231 (4) (2012) 1499–1523.